Ab initio molecular dynamics: Propagating the density matrix with Gaussian orbitals. III. Comparison with Born–Oppenheimer dynamics

H. Bernhard Schlegel
Department of Chemistry, Wayne State University, Detroit, Michigan 48202-3489

Srinivasan S. Iyengar
Department of Chemistry and Henry Eyring Center for Theoretical Chemistry, University of Utah, Salt Lake City, Utah 84112-0850

Xiaosong Li and John M. Millam
Department of Chemistry, Wayne State University, Detroit, Michigan 48202-3489

Gregory A. Voth
Department of Chemistry and Henry Eyring Center for Theoretical Chemistry, University of Utah, Salt Lake City, Utah 84112-0850

Gustavo E. Scuseria
Department of Chemistry and Center for Nanoscale Science and Technology, Rice University, Houston, Texas 77005-1892

Michael J. Frisch
Gaussian Inc., North Haven, Connecticut 06473-1712

(Received 3 May 2002; accepted 26 August 2002)

In a recently developed approach to *ab initio* molecular dynamics (ADMP), we used an extended Lagrangian to propagate the density matrix in a basis of atom centered Gaussian functions. Results of trajectory calculations obtained by this method are compared with the Born–Oppenheimer approach (BO), in which the density is converged at each step rather than propagated. For NaCl, the vibrational frequency with ADMP is found to be independent of the fictitious electronic mass and to be equal to the BO trajectory result. For the photodissociation of formaldehyde, $H_2CO \rightarrow H_2 + CO$, and the three body dissociation of glyoxal, $C_2H_2O2 \rightarrow H_2 + 2CO$, very good agreement is found between the Born–Oppenheimer trajectories and the extended Lagrangian approach in terms of the rotational and vibrational energy distributions of the products. A 1.2 ps simulation of the dynamics of chloride ion in a cluster of 25 water molecules was used as a third test case. The Fourier transform of the velocity–velocity autocorrelation function showed the expected features in the vibrational spectrum corresponding to strong hydrogen bonding in the cluster. A redshift of approximately 200 cm^{-1} was observed in the hydroxyl stretch due to the presence of the chloride ion. Energy conservation and adiabaticity were maintained very well in all of the test cases. [DOI: 10.1063/1.1514582]

I. INTRODUCTION

Direct classical trajectory calculations can be grouped into two major categories: Born–Oppenheimer (BO) methods and extended Lagrangian (EL) molecular dynamics.[1–7] For the former, each time that information about the potential energy surface is needed, the electronic structure calculation is fully converged. In the latter approach, as exemplified by the Car–Parrinello (CP) method,[2] the wave function is propagated along with the classical nuclear degrees of freedom. This is achieved by using an extended Lagrangian procedure[8,9] and by adjusting the relative time scales of the electronic and nuclear motions. Traditionally, the CP approach employs plane-wave basis sets and uses Kohn–Sham orbitals (however, Gaussian orbitals have been found to be useful adjunct[10,11]). Recently, we have developed the theory and code for an extended Lagrangian molecular dynamics trajectory method that employs atom-centered basis functions and density matrix propagation (ADMP).[12,13] This approach is well suited for the dynamics of chemical systems such as clusters and gas-phase reactions. Because it is based on linear scaling DFT code,[14] the calculations will scale as O(N) for large systems. For condensed phases, our code is being extended to periodic boundary condition calculations that employ atom centered functions.[15] For large biological systems, the current method is also being expanded to include QM/MM treatments.[16]

Some of the specific advantages of the ADMP method include (i) the freedom to rigorously treat all electrons in the system or to use pseudopotentials, (ii) the capability of using reasonably large time-steps through the use of a tensorial fictitious mass with smaller values for the fictitious mass (among other things, allows one to retain hydrogen atoms in the system and not substitute heavier isotopes), (iii) the latitude to employ a wide variety of accurate and effective exchange-correlation functionals, including hybrid density functionals and kinetic energy functionals, (iv) the ability to treat charged molecular systems and clusters[17] which is ex-

pected to be an important advantage in treating QM/MM systems[16] (calculations of molecular clusters are nontrivial in most implementations of the plane-wave Car–Parrinello method because systems are treated as periodic[7,18,19]), (v) rigorous on-the-fly control of the deviation from the Born–Oppenheimer surface and the mixing of fictitious and real kinetic energies, and (vi) good computational efficiency due to the use of fewer basis functions per atom, larger time steps, and asymptotic O(N) scaling using established techniques.[14]

Because the electronic structure is propagated in the extended Lagrangian approach rather than converged, the potential energy surface has an implicit error that is proportional to the maximum fictitious kinetic energy of the electronic degrees of freedom. In turn, this kinetic energy is proportional to the fictitious mass. However, for reasonable values of the fictitious mass, the electronic structure oscillates about the converged wave function, and the forces on the nuclei should average to the values obtained from the converged calculations.[7] Hence EL dynamics yields results that are very similar to BO dynamics. A further complication with the EL approach is the possibility of energy flowing between the nuclear and electronic degrees of freedom. This is primarily controlled by choosing the fictitious electronic mass so that the time scale for the electronic structure propagation is an order of magnitude faster than the nuclear motions. Nosé–Hoover chain thermostats[20–22] have also been used in the Kohn–Sham orbital based plane-wave implementation of the Car–Parrinello method to control the adiabaticity.

In the initial tests of our ADMP approach, we examined a number of individual trajectories and found that the coordinates and velocities obtained with the ADMP method agreed very well with accurate BO trajectories.[12] We have also studied the effect of step-size and fictitious electronic mass on the energy conservation and adiabaticity of the ADMP calculations, and have shown that the deviation of the ADMP trajectory from the BO trajectory is directly proportional to the magnitude of the fictitious mass.[13] In particular, we found that with time steps comparable to plane-wave CP calculations, we can use a smaller fictitious electronic mass and lighter nuclei (e.g., hydrogen instead of deuterium in the simulation of water), and still maintain good energy conservation and adiabaticity without resorting to thermostats. This is a consequence of the fact that the changes in coefficients are much smaller when electronic distribution is expressed in terms of (local) atom-centered functions rather than (global) plane waves. Hence, smaller fictitious electronic masses can be used in the present scheme, thereby naturally improving the adiabaticity and energy conservation of our method.

Our method may be contrasted with other extended Lagrangian approaches that use Gaussian basis sets. Within the generalized valence bond (GVB)[23,24] and Hartree–Fock[25] framework, Gaussian basis functions have been used in the propagation of the orbital and wave function coefficients. However, the past schemes have had some difficulty with energy conservation.[23] In general, the forces on the nuclei are calculated as the negative of the derivative of the expectation value of the Hamiltonian with respect to the nuclear positions. These derivatives have contributions from the derivative of the Hamiltonian (the Hellmann–Feynman term) and derivatives of the wave function (for converged wave functions these terms are sometimes referred to as the ''Pulay'' forces[26] in quantum chemistry),

$$\partial E/\partial \mathbf{R} = \langle \Psi | \partial H/\partial \mathbf{R} | \Psi \rangle + \langle \partial \Psi/\partial \mathbf{R} | H | \Psi \rangle + \langle \Psi | H | \partial \Psi/\partial \mathbf{R} \rangle. \quad (1)$$

In the plane-wave implementation of the Car–Parrinello approach, the Pulay terms are zero because the basis set does not depend on the nuclear coordinates. However, if the wave function is constructed using a finite number of atom-centered basis functions, the Pulay terms do not vanish. The relatively lower degree of energy conservation found in Refs. 23–25 may be due to the use of only the Hellman–Feynman forces.[27] In our formulation,[12,13] we included the Pulay forces as well as the Hellman–Feynman forces. We have also included additional terms that arise from the fact that the Hamiltonian matrix (for DFT, Hartree–Fock or any semiempirical scheme) and the electronic density matrix do not commute, since the system is not exactly on the Born–Oppenheimer surface within this extended Lagrangian scheme. As can be seen from Refs. 12 and 13, energy conservation and adiabaticity are well controlled in the present method.

Floating Gaussian orbitals have also been used[28] in a CP scheme in which the widths, centers and coefficients are used as dynamic variables. The structure and dynamics of an alkali metal atom in rare gas clusters were investigated by representing the single valence electron of the metal by a set of 5–9 independently floating Gaussians. However, for general systems involving multiple electrons and undergoing chemical reactions, it may be difficult to know *a priori* which regions may have important density contributions and fluctuations during the course of a simulation. With atom-centered Gaussian basis functions, the electron density follows the nuclear framework and there is no ambiguity in representing the electronic structure of molecular systems.

Theoretical and computational aspects of energy conservation and adiabatic control in our ADMP scheme were discussed in our previous report.[13] In a recent paper, Tangney and Scandolo[29] have derived similar expressions for the difference between the forces used in CP and BO simulations. Furthermore, they find that for systems with large electron-ion coupling, plane-wave CP calculations have a systematic bias proportional to the fictitious electronic mass. These problems in the CP approach can be overcome by rescaling the ion masses and by correcting the forces with a rigid ion approximation. In the present approach, we use atom-centered functions to represent the density matrix. The forces calculated for the nuclei already take into account the fact that the functions follow the nuclei (i.e., the Pulay forces, as discussed earlier), and the fictitious mass pertains only to the adjustment of the density around the nuclear position. As illustrated by some of the examples in the present paper, our ADMP scheme has no systematic bias due to the fictitious electronic mass in computing properties such as vibrational frequencies.

In the present paper, we have undertaken a more detailed comparison of the dynamical properties obtained with ADMP and BO trajectory calculations. Specifically, we have examined the vibration of an ionic system, have studied the product energy distributions for the photodissociation of formaldehyde and the three-body dissociation of glyoxal, and have calculated the vibrational spectrum of a cluster of 25 water molecules solvating a chloride ion.

II. THE ATOM-CENTERED DENSITY MATRIX PROPAGATION (ADMP) USING AN EXTENDED LAGRANGIAN APPROACH

Details of the ADMP method have been described in our earlier papers;[12,13] only a brief outline is given in this section. Like density matrix search methods for calculating electronic energies,[30] the equations for propagation of the density matrix are simplest in an orthonormal basis (e.g., Löwdin or Cholesky orthonormalization). For ADMP the Lagrangian for the system can be written as

$$\mathcal{L}=\tfrac{1}{2}\mathrm{Tr}[\mathbf{V}^T\mathbf{M}\mathbf{V}]+\tfrac{1}{2}\mathrm{Tr}[\{\boldsymbol{\mu}^{1/4}\mathbf{W}\boldsymbol{\mu}^{1/4}\}^2] - E(\mathbf{R},\mathbf{P})-\mathrm{Tr}[\Lambda(\mathbf{PP}-\mathbf{P})], \tag{2}$$

where **R**, **V**, and **M** are the nuclear positions, velocities and masses; **P** and **W** are the density matrix and the density matrix velocity. The fictitious mass for the electronic degrees of freedom, $\boldsymbol{\mu}$, is chosen as a diagonal matrix with larger values for the core orbitals ($\mu_{\mathrm{core}}^{1/2}=\mu_{\mathrm{valence}}^{1/2}\ [2|F_{ii}+2|^{1/2}+1]$ for $F_{ii}<-2$, where F_{ii} is the diagonal Fock matrix element).[11] Constraints on the total number of electrons and the idempotency of the one particle density matrix enforce *N*-representability and are imposed using the Lagrangian multiplier matrix Λ. The energy is calculated using the McWeeny purification of the density,[31] $\tilde{\mathbf{P}}=3\,\mathbf{P}^2-2\,\mathbf{P}^3$. The Euler–Lagrange equations of motion are

$$\mathbf{M}\,\mathrm{d}^2\mathbf{R}/\mathrm{d}t^2=-\partial E/\partial\mathbf{R}|_{\mathbf{P}}, \qquad \mathrm{d}^2\mathbf{P}/\mathrm{d}t^2=-\boldsymbol{\mu}^{-1/2}[\partial E/\partial\mathbf{P}|_{\mathbf{R}}+\boldsymbol{\Lambda}\mathbf{P}+\mathbf{P}\boldsymbol{\Lambda}-\boldsymbol{\Lambda}]\boldsymbol{\mu}^{-1/2}. \tag{3}$$

These can be integrated using the velocity Verlet algorithm[32,33]

$$\begin{aligned}\mathbf{P}_{i+1}&=\mathbf{P}_i+\mathbf{W}_i\Delta t-\boldsymbol{\mu}^{-1/2}[\partial E(\mathbf{R}_i,\mathbf{P}_i)/\partial\mathbf{P}|_{\mathbf{R}}+\boldsymbol{\Lambda}_i\mathbf{P}_i+\mathbf{P}_i\boldsymbol{\Lambda}_i-\boldsymbol{\Lambda}_i]\boldsymbol{\mu}^{-1/2}\Delta t^2/2,\\ \mathbf{W}_{i+1/2}&=\mathbf{W}_i-\boldsymbol{\mu}^{-1/2}[\partial E(\mathbf{R}_i,\mathbf{P}_i)/\partial\mathbf{P}|_{\mathbf{R}}+\boldsymbol{\Lambda}_i\mathbf{P}_i+\mathbf{P}_i\boldsymbol{\Lambda}_i-\boldsymbol{\Lambda}_i]\boldsymbol{\mu}^{-1/2}\Delta t/2\\ &=[\mathbf{P}_{i+1}-\mathbf{P}_i]/\Delta t,\\ \mathbf{W}_{i+1}&=\mathbf{W}_{i+1/2}-\boldsymbol{\mu}^{-1/2}[\partial E(\mathbf{R}_{i+1},\mathbf{P}_{i+1})/\partial\mathbf{P}|_{\mathrm{R}}+\boldsymbol{\Lambda}_{i+1}\mathbf{P}_{i+1}+\mathbf{P}_{i+1}\boldsymbol{\Lambda}_{i+1}-\boldsymbol{\Lambda}_{i+1}]\boldsymbol{\mu}^{-1/2}\Delta t/2.\end{aligned} \tag{4}$$

The Lagrangian multiplier matrices are determined by an iterative scheme[12,13] so that $\mathbf{P}_{i+1}$ and $\mathbf{W}_{i+1}$ satisfy the idempotency constraint, $\mathbf{P}^2=\mathbf{P}$, and its time derivative, $\mathbf{PW}+\mathbf{WP}=\mathbf{W}$. In calculating $\partial E/\partial\mathbf{R}|_{\mathbf{P}}$ one needs to take into account that **P** is not converged and that the transformation between the nonorthogonal atomic orbital basis and the orthonormal basis depends on **R**. This leads to a somewhat more complicated expression than used for gradients of converged SCF energies.[12] An important factor in the viability of this approach is that we have been able to obtain the derivative of the transformation matrix in closed form for both Löwdin and Cholesky orthonormalization.[12]

In the present formalism, the basis functions are orthonormal, but they depend upon the instantaneous nuclear positions. Hence, the basis functions may be considered to be ''traveling'' along with the (classical) nuclear coordinates. This is to be contrasted with standard implementations of the original Car–Parrinello methodology, where the electronic degrees of freedom are represented in terms of the (globally fixed) plane-wave basis functions. The present framework of basis functions may also be compared with various approaches[6,34,35] in quantum scattering theory, where quantum dynamics is studied using traveling basis sets. The difference here is the ''traveling'' nature of our basis functions arise from a classical propagation of the nuclear positions, using a third-order Trotter factored (classical) Liouville propagator (i.e., the velocity Verlet integrator). Travelling, localized basis functions, such as wavelets, have also found great use in the fields of digital signal processing[36] and computational fluid dynamics.[37]

The accuracy of the velocity Verlet method and other symplectic integrators for trajectory integration continues to be a topic of investigation (see Refs. 38–40 and references therein). Conservation of energy has often been used to assess the quality of classical trajectory calculations. It is well known that integration by velocity Verlet is accurate to third order. Fluctuations in the total energy for velocity Verlet integrations, on the contrary, are larger than the quality of the dynamics would suggest and have been shown to be second order in time.[38–40] This has been attributed to the use of low order interpolation methods in computing the kinetic energy.[40] For a harmonic oscillator, Mazur[40] has shown that the fluctuations in the total energy are proportional to $\omega^2\,\Delta t^2$ times the magnitude of the potential (or kinetic) energy. In ADMP, after equilibration, the nuclear and density degrees of freedom behave adiabatically, i.e., like uncoupled degrees of freedom. The fictitious mass is chosen so that the density oscillations are an order of magnitude higher than the highest frequency nuclear motions; however, the equilibrated kinetic energy of the density is about two orders of magnitude lower than the kinetic energy of the nuclei. Hence, for a given stepsize, the error in the conservation of energy for the ADMP and BO methods should be comparable and proportional to $\omega^2\,\Delta t^2$ times the magnitude of the potential (or kinetic) energy of the nuclei, where ω is the fastest nuclear degree of freedom. Thus, the step sizes and fictitious masses chosen for the simulations discussed below should yield satisfactory nuclear dynamics. The comparisons with Born–Oppenheimer dynamics bear this out.

III. EFFECT OF THE FICTITIOUS MASS ON VIBRATIONAL FREQUENCIES

In a study using plane-wave CP simulations, Tangney and Scandolo[29] found a systematic bias in the phonon frequency of crystalline MgO as the fictitious electronic mass was varied. Since this system is very ionic, there is strong

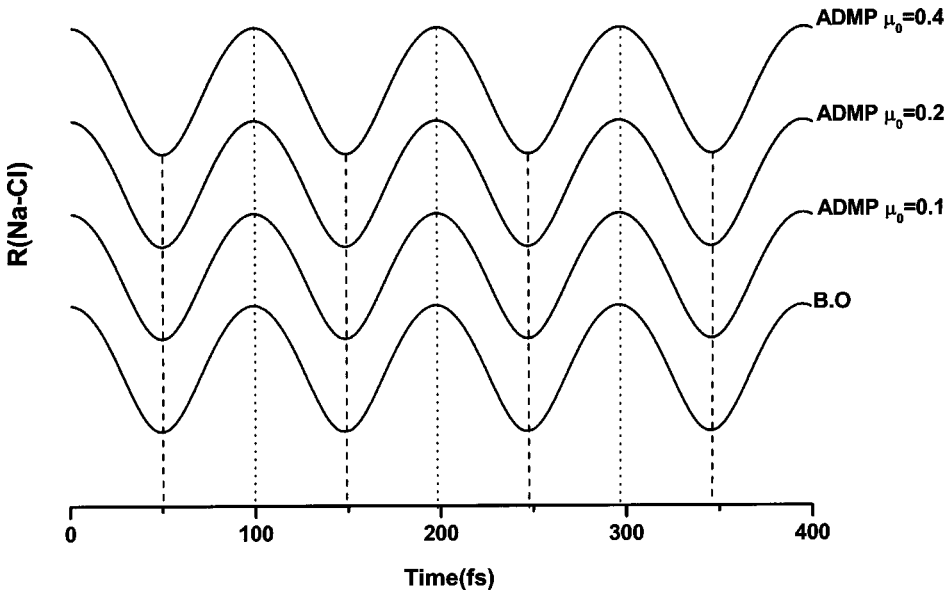

FIG. 1. Vibration of diatomic NaCl computed using the Born–Oppenheimer approach and with the ADMP method using different values for the fictitious electronic mass (μ_{valence} in amu bohr^2).

coupling between the electrons and the nuclei. The resulting errors in the CP dynamics can be partially corrected by using a rigid ion approximation. In this case, the effective mass of a moving ion has contributions from the fictitious mass of the electrons as well as the mass of the nucleus. Thus, the effective mass of the ion changes as the fictitious electronic mass is varied. Tangney and Scandolo[29] showed that this problem can be overcome by rescaling the ion masses by a value that depends on the fictitious electronic mass and on the degree of coupling between the nucleus and the electrons.

Since the dependence on the fictitious mass is most pronounced in ionic systems, we have chosen diatomic NaCl as a simple example to study whether our ADMP scheme handles these problems correctly. Note that an all electron calculation on NaCl is a more difficult test of the effect of the fictitious mass of the electrons, since NaCl is more ionic and has more core electrons with large μ. Figure 1 illustrates the vibration of NaCl computed with the BO approach and with our ADMP using $\mu_{\text{valence}}=0.1$, 0.2, and 0.4 amu bohr^2 (ca. 182, 364, and 728 a.u., respectively) and a time step of 0.1 fs. Calculations were carried out at the Hartree–Fock level of theory using the 3-21G all electron basis, with core functions weighted more heavily than valence functions, as described in Sec. II and in more detail in Ref. 13. It is readily apparent from Fig. 1 that the vibrational frequency does not depend on the fictitious mass and that the ADMP results are the same as the BO trajectory. This is true for the present method even for larger fictitious masses and for a more ionic system than tested in Ref. 29 in the plane-wave CP implementation. The fact that fundamental properties such as vibrational frequencies are independent of the fictitious mass is an important advantage of our ADMP scheme for investigating the dynamics of chemical systems.

IV. FORMALDEHYDE PHOTODISSOCIATION

The dynamics of $H_2CO \rightarrow H_2 + CO$ photodissociation have been extensively studied both experimentally[41–51] and theoretically,[52–67] and thus serves as an excellent test case. After excitation to the S_1 state, formaldehyde undergoes rapid internal conversion, returning to the ground state with a high degree of vibrational excitation. Photolysis at 29 500 cm^{-1} yields H_2 and CO as the only products. Hydrogen molecule is produced rotationally cold but with considerable vibrational excitation. Carbon monoxide shows very little vibrational excitation but has a broad rotational energy distribution with $\langle J \rangle = 42$. Classical trajectory calculations with high quality fitted surfaces[65,67] and Born–Oppenheimer *ab initio* molecular dynamics[68,69] are able to reproduce the product vibrational and rotational energy distributions. By contrast, it has been demonstrated that semiempirical electronic structure methods are unable to reproduce the product energy distributions.[66]

Classical trajectories were calculated using the development version of the Gaussian series of programs[70] using the HF/3-21G and HF/6-31G(d,p) levels of theory. For each case, 200 trajectories were started from the transition state and integrated toward products. The reaction coordinate was given 5.1 kcal/mol kinetic energy, corresponding to the difference between the photolysis energy and the barrier height. Zero point energy was added to the remaining vibrational coordinates, and the phase of the vibrational motion was chosen randomly. The initial total angular momentum was chosen to be zero. Both the BO and ADMP trajectories for a given level of theory were started from the same ensemble of initial coordinates and velocities. The BO trajectory results employed a Hessian-based predictor–corrector integration scheme[71] with Hessian updating[72] and are comparable to previous studies.[68,69] A step size of 0.25 amu$^{1/2}$ bohr was used and the Hessian was updated for five steps before being recalculated analytically. The ADMP trajectories were integrated with a step size of 0.1 fs and used μ_{valence} ranging from 0.025 to 0.40 amu bohr^2 for the fictitious mass for the electronic degrees of freedom.

Figure 2 compares the conservation of energy and adiabaticity for various choices of the fictitious mass for one

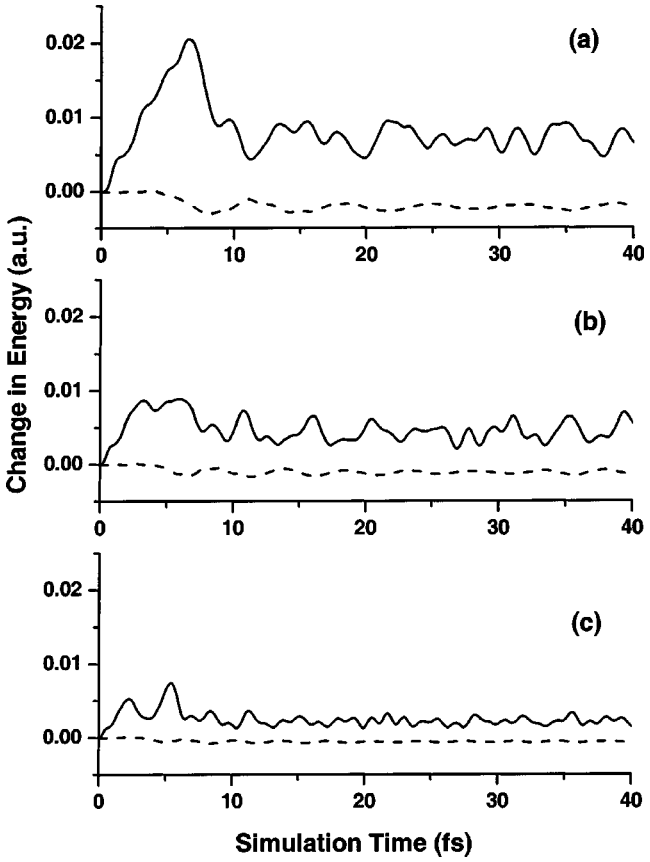

FIG. 2. Effect of fictitious mass used in the ADMP trajectories on energy conservation and adiabaticity for a H_2CO photodissociation trajectory: total energy (dashed line) and kinetic energy of the density (solid line), μ_{valence} = (a) 0.40, (b) 0.20, and (c) 0.10 amu bohr^2, $\Delta t = 0.1$ fs.

trajectory in the photodissociation of H_2CO. The total energy is conserved to 0.0007, 0.0017, and 0.003 hartree for $\mu_{\text{valence}} = 0.1$, 0.2, and 0.4 amu bohr^2, respectively. As discussed in Sec. II, the dynamics is more accurate than what the total energy conservation suggests as will be evident from the product distributions discussed below. Because the trajectories are started with zero kinetic energy for the density, initially there is some transfer of energy from the nuclear motion to the electronic degrees of freedom. However, after this short equilibration time, there is no drift in the components of the energy, indicating that adiabaticity is being maintained satisfactorily. As can be seen from Fig. 2, these fluctuations in the kinetic energy of the density are roughly proportional to the fictitious mass used for the integration. This aspect is consistent with our analytical results[13] which show that the fluctuations are bounded by an amount proportional to the fictitious mass and that they go to zero as the fictitious mass goes to zero, recovering the Born–Oppenheimer case. However, obtaining this limit is not practical from a computational point, since the time step size must also be reduced to ensure accurate integration of the electronic degrees of freedom. Thus the extended Lagrangian approach (both CP and ADMP) requires a compromise between accuracy in the calculated potential energy and efficiency of the trajectory integration. For the very rapid dissociation reactions of formaldehyde and glyoxal (see below), we choose a maximum fictitious mass of $\mu_{\text{valence}} = 0.10$ amu bohr^2 (182 a.u.). The power of the present method lies in using smaller values for the fictitious mass along with reasonably large time steps. In a subsequent paper, we will examine further the theoretical basis for the connection between the magnitude of the fictitious mass and deviations from the Born–Oppenheimer surface, gauged by the magnitude of the commutator of the Hamiltonian and the density matrix.[73]

The calculated and experimental vibrational energy distributions are compared in Table I. As noted previously, the degree of vibrational excitation of H_2 varies with the level of theory, and depends on the amount of energy released in the portion of the reaction path where most of the H–H bond length changes occur.[69] For a given level of theory, the ADMP and BO trajectories produce the same picture: CO is almost all in $v=0$, and H_2 largely in $v=1$ but with sizable populations in $v=0$ and $v=2$. The agreement is quite satisfactory, particularly for the HF/6-31G(d,p) level of theory. As a further test of the effect of the fictitious mass on the observables, we varied μ_{valence} from 0.025 to 0.1 amu bohr^2.

TABLE I. Vibrational energy distribution for the H_2 and CO products of H_2CO photodissociation.

	CO		H_2			
Level	$v=0$	$v=1$	$v=0$	$v=1$	$v=2$	$v=3$
BO trajectories						
HF/3-21G	92	8	28	37	18	13
HF/6-31G(d,p)	89	11	37	35	20	8
MP2/6-311G(d,p)	87	13	30	34	27	9
B3LYP/6-311G(d,p)	93	7	43	34	21	2
ADMP trajectories						
HF/CEP-31G	79	21	27	42	25	6
HF/3-21G	92	8	22	37	24	14
HF/6-31G(d,p)[a]	87	13	36	35	20	9
HF/6-31G(d,p)[b]	88	12	37	35	20	8
HF/6-31G(d,p)[c]	88	13	37	35	21	7
Experiment	88	12	24	41	25	9

[a]0.025 amu bohr^2 electron fictitious mass.
[b]0.05 amu bohr^2 electron fictitious mass.
[c]0.10 amu bohr^2 electron fictitious mass.

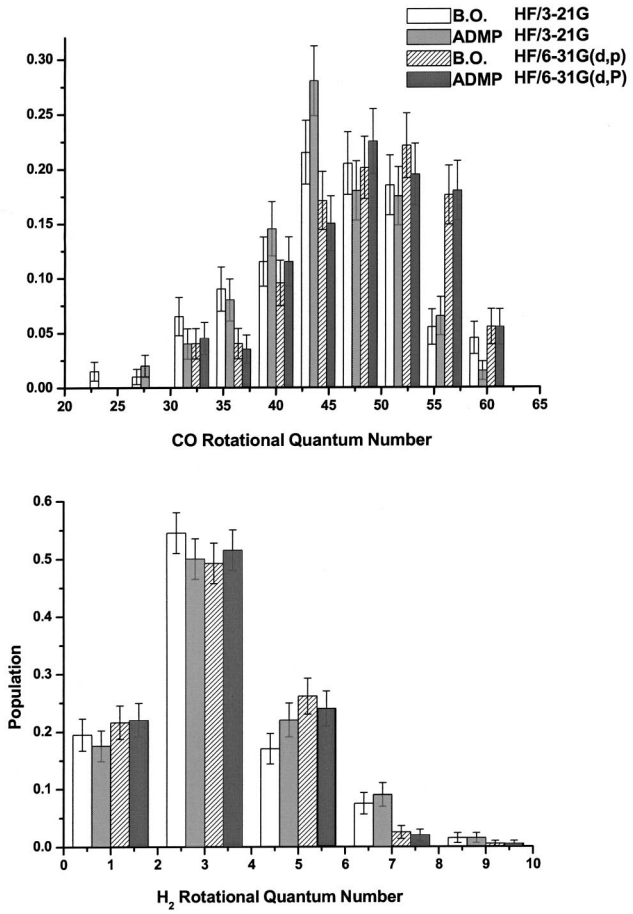

FIG. 3. Comparison of the rotational energy distributions for the H_2 and CO products of H_2CO photodissociation, computed using BO and ADMP trajectories ($\mu_{\text{valence}}=0.025$ amu bohr^2) with the HF/3-21G and HF/6-31G(d,p) levels of theory.

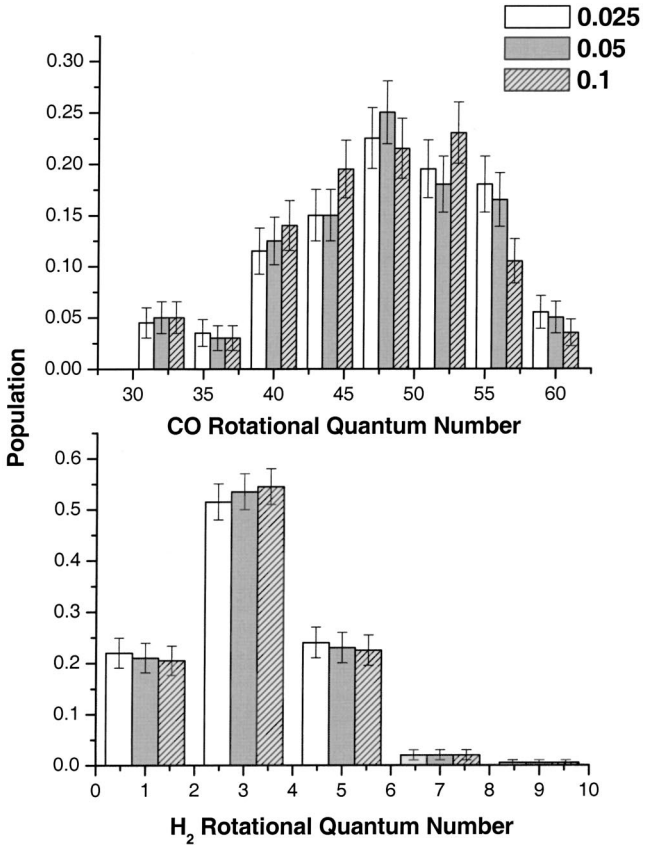

FIG. 4. Effect of fictitious mass (μ_{valence}, amu bohr^2) used in the ADMP HF/6-31G(d,p) trajectories on the rotational energy distributions for the CO and H_2 products of H_2CO photodissociation.

The changes in the vibrational populations of the products are at most $\pm 1\%$.

The rotational energy distributions are compared in Fig. 3. All of the levels of theory predict the CO distribution to be broad with a large $\langle J\rangle$ and the H_2 distribution to be cold. The ADMP ($\mu_{\text{valence}}=0.025$ amu bohr^2) and BO trajectories are in very good agreement for H_2; the differences are a bit larger for CO but are within the error bars. The average rotational energies are essentially the same [for CO, $\langle J\rangle = 48.5$ for BO and 48.2 for ADMP at HF/6-31G(d,p)] but the distributions are slightly different. This may be the result of the fluctuations in ADMP energies away from the Born–Oppenheimer surface. Figure 4 shows the effect of increasing μ_{valence} from 0.025 to 0.050 to 0.10 amu bohr^2; the distributions shift somewhat, but $\langle J\rangle$ remains nearly constant (for CO, $\langle J\rangle = 48.2$, 47.9, and 47.1, respectively).

V. THREE-BODY DISSOCIATION OF GLYOXAL

The photofragmentation of glyoxal, $C_2H_2O_2$, is one of the best studied examples of a synchronous three-body fragmentation (see Ref. 74 for a summary of the experimental work). Intersystem crossing from the first excited state, S_1, is induced by collisions and the triplet dissociates to $H_2CO + CO$. However, under collisionless conditions, the lifetime of S_1 is 10^{-6} s, and about 50% returns to the ground state by internal conversion. The vibrationally excited ground state has enough energy to dissociate via three channels

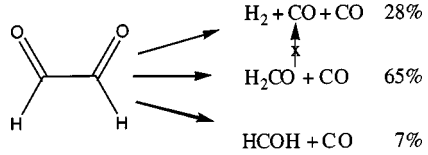

Hepburn *et al.*[75] have measured the branching ratios for the three channels. Houston and co-workers have determined that CO is formed almost entirely in the vibrational ground state but with a broad rotational distribution,[76] and have observed that H_2 is formed in $v=1$ with $J=1-9$.[74] Early calculations established the ''triple whammy'' transition state as a synchronous three-body fragmentation,[77–79] and energetic considerations ruled out that these products could come from the H_2CO+CO channel by secondary fragmentation of H_2CO. Recent calculations[80,81] have firmly established the transition states and barrier heights for all three channels, and the activation energies are in agreement with the photofragmentation branching ratios[75] and the thermal unimolecular decomposition rates.[82]

Similar to the formaldehyde dissociation discussed above, ca. 200 trajectories were integrated for each of the levels of theory starting from the optimized transition state

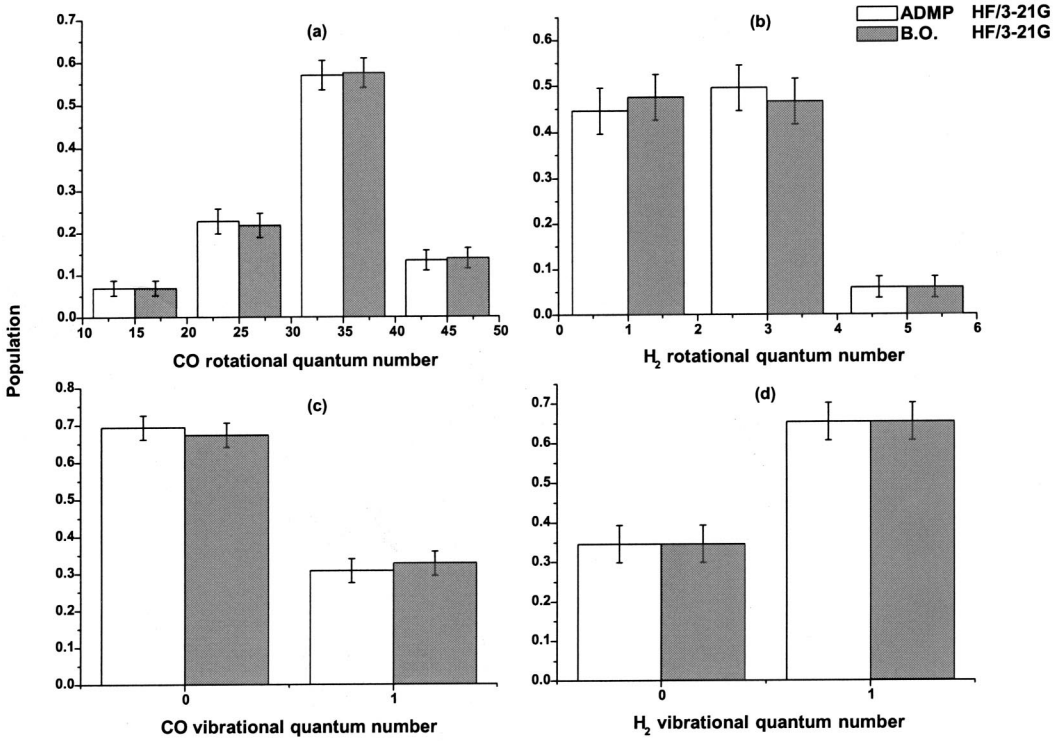

FIG. 5. Comparison of the rotational and vibrational energy distributions for the CO and H_2 products of glyoxal three body dissociation, computed using BO and ADMP trajectories with the HF/3-21G level of theory.

for three-body fragmentation. To simulate the experimental photolysis of glyoxal, the initial conditions where chosen to correspond to a microcanonical ensemble with 4 kcal/mol energy above the zero point energy of the transition state and with zero angular momentum. The BO trajectory results were reported previously,[83] and make use of the Hessian-based predictor–corrector method with updating[71,72] described in the preceding section. The ADMP trajectories were started with the same initial coordinates and velocities, and used a step size of 0.1 fs with a fictitious mass $\mu_{\text{valence}} = 0.025$ amu bohr^2 for the electronic degrees of freedom; this gives around 2×10^{-4} hartree for the conservation of the total energy.

Figure 5 compares the energy distributions for the three-body dissociation of glyoxal obtained with ADMP and BO trajectory methods. For the vibrational energy distributions computed at the HF/3-21G level, the agreement between the two methods is excellent. Higher levels of theory lead[84] to lower levels of vibrational excitation more in line with experiment.[74] The comparison between the ADMP and BO methods is also very good for the rotational energy distributions, with the differences being well within the error bars.

VI. DYNAMICS OF $(H_2O)_{25}Cl^-$

A cluster containing a chloride ion surrounded by 25 water molecules has been used as a test case in our previous work.[10,11] In the present study, we use this system to compare the performance of the ADMP method with the BO method by first testing the energy conservation in these methods, and then by analyzing the O–H vibrational stretching frequencies obtained from dynamical simulations using both these methods. The initial performance comparisons were carried out using the PBE[85,86] density functional and the 3-21G* basis set. We have integrated this system for 1.2 ps using the ADMP scheme, with the core functions weighted more heavily than valence functions, as described in Sec. II and in more detail in Ref. 13. Trajectories were started from the MM3 optimized geometry. The velocities of the individual atoms were chosen randomly (to simulate a Boltzmann distribution) such that the total initial nuclear kinetic energy was 0.1 hartree. The initial density matrix velocity was chosen to be zero. The system was allowed to equilibrate for 300 fs using ADMP, and the result was used as the initial state for further study. This same initial state (i.e., the nuclear coordinates and velocities from the ADMP calculation after equilibration) was also used for the Born–Oppenheimer dynamics simulations. To facilitate a direct comparison with the ADMP trajectory, the BO trajectory was integrated using the velocity Verlet method (the Hessian based integration scheme that was efficient for smaller systems such as formaldehyde and glyoxal, becomes more expensive than gradient based integration for larger systems). In Fig. 6 we present the degree of energy conservation for various time steps for the BO method. The substantial drift at $\Delta t = 1.5$ fs and the wildly oscillatory nature of the $\Delta t = 1.0$ fs BO simulations indicate that these time steps are too large. A time step between 0.5–0.75 fs is a safer value for BO dynamics, a choice that is supported by the large number of water simulations in the literature using parametrized models, that generally use time steps in the range of 0.5 fs (for example, see Ref. 87). Larger time-steps generally exhibit poorer energy conservation since the velocity Verlet integration scheme has an error that is

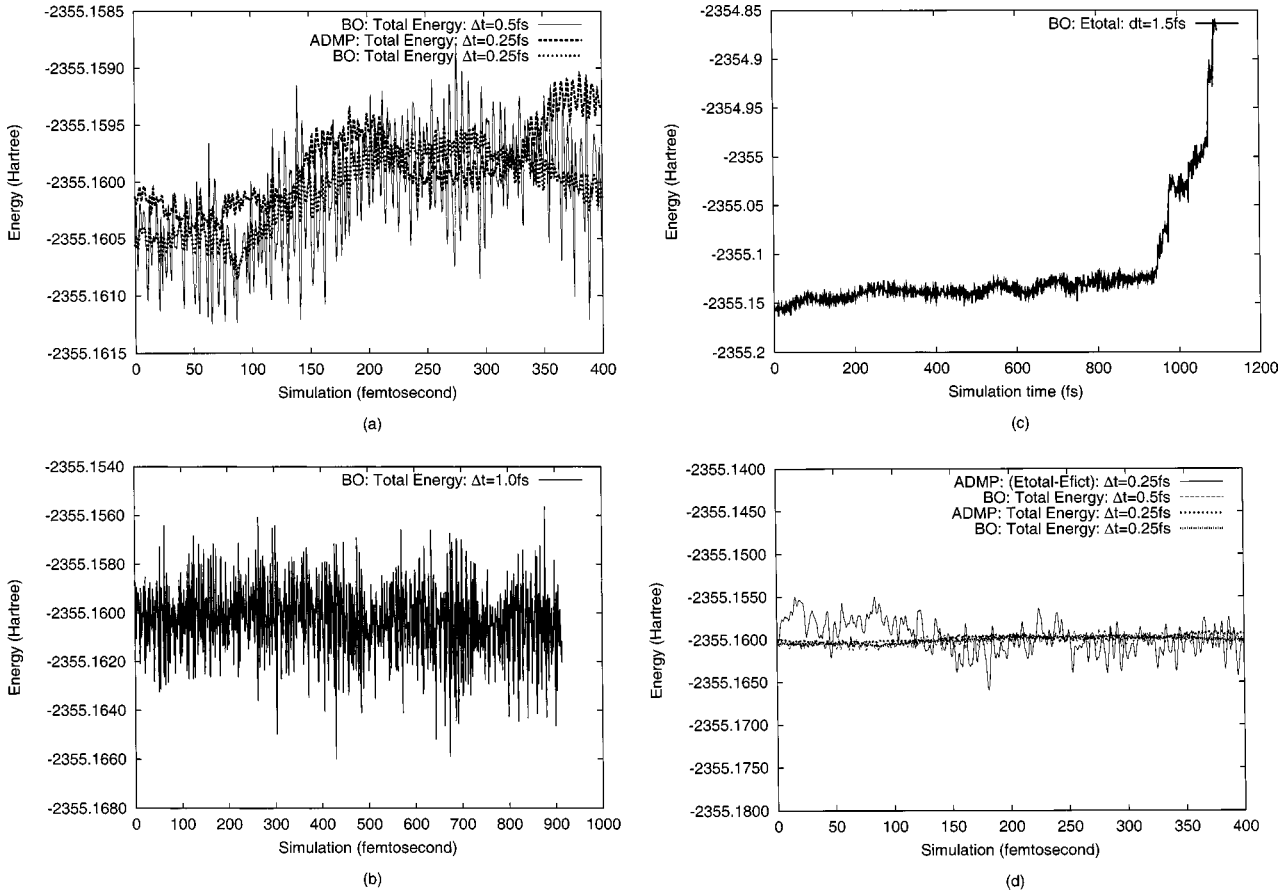

FIG. 6. Energy conservation for simulations of $Cl^-(H_2O)_{25}$ at the PBE/3-21G* level of theory. (a) ADMP with $\Delta t = 0.25$ fs and BO with $\Delta t = 0.25, 0.50$ fs, (b) BO with $\Delta t = 1.00$ fs, (c) BO with $\Delta t = 1.50$ fs, and (d) comparison of $E_{\text{total}} - E_{\text{fict}}$ and E_{total} (see text for details).

proportional to Δt^3. Figure 6(d) also illustrates the degree of energy conservation and adiabatic control obtained when a time step of 0.25 fs is used with the ADMP scheme ($\mu_{\text{valence}} = 0.1$ amu bohr^2 or approximately 182 a.u.). The total energy conservation for the ADMP scheme is very similar to that seen in the BO scheme with time step 0.25 fs. In addition we also present the difference between the total energy and the fictitious kinetic energy for ADMP ($E_{\text{total}} - E_{\text{fict}}$). This quantity has been described in our previous work[12,13] and in the CP community[4] as the ''real'' energy. As is generally expected[4] this ''real'' energy does oscillate about the true BO energy [see Fig. 6(d)] when identical initial conditions for nuclear positions and velocities are used. However, it is important to note that the quantity ($E_{\text{total}} - E_{\text{fict}}$), is not in general the actual energy surface on which the nuclei move, since the electronic energy is not the corresponding converged quantity.

One measure of the quality of integration in dynamics is the conservation of the total energy of the system (however, see Sec. II and Refs. 38–40, for a discussion suggesting that the quality of velocity Verlet dynamics is generally better than indicated by the total energy conservation). In our case, the energy conservation for ADMP at 0.25 fs is in fact as good as the conservation of energy for BO at 0.25 fs. The energy conservation for BO at 0.5 fs is somewhat worse than the corresponding value for ADMP at 0.25 fs, but is still sufficiently accurate. Figure 6(d) shows that the fluctuations in ($E_{\text{total}} - E_{\text{fict}}$) have an rms deviation of 1.3 kcal/mol (0.002 Hartree). The average of ($E_{\text{total}} - E_{\text{fict}}$) is within 0.2 kcal/mol of the average BO energy at 0.5 fs, and fluctuates about the BO energy by ca. 1.5 kcal/mol. In ADMP, the system is not actually on the BO surface, but oscillates about this surface due to the fictitious kinetic energy, and in an average sense has the same properties as would a trajectory converged to the BO surface at every instant. While the oscillatory nature of the fictitious kinetic energy is not guaranteed in general, we have discussed in Ref. 13 the conditions under which this oscillatory behavior can be maintained. The fluctuations in ($E_{\text{total}} - E_{\text{fict}}$) may be reduced further by decreasing the fictitious mass and the time step. However, the results of the ADMP trajectory at 0.25 fs are already in good agreement with the BO trajectory. Finally, the oscillations in ($E_{\text{total}} - E_{\text{fict}}$) do not reflect the quality of the dynamics, since it is not a conserved quantity but only a part of the full ADMP Hamiltonian.

In the present implementation, ADMP is about 3–4 times faster than the BO approach with the same time step. For each step, BO typically requires 8–12 SCF cycles (although many more cycles may be needed for difficult cases such as transition metal complexes). The ADMP scheme requires the equivalent of one SCF cycle to evaluate $\partial E/\partial P|_R$ and the electronic energy. Both methods evaluate the gradients of the energy with respect to the nuclear coordinates,

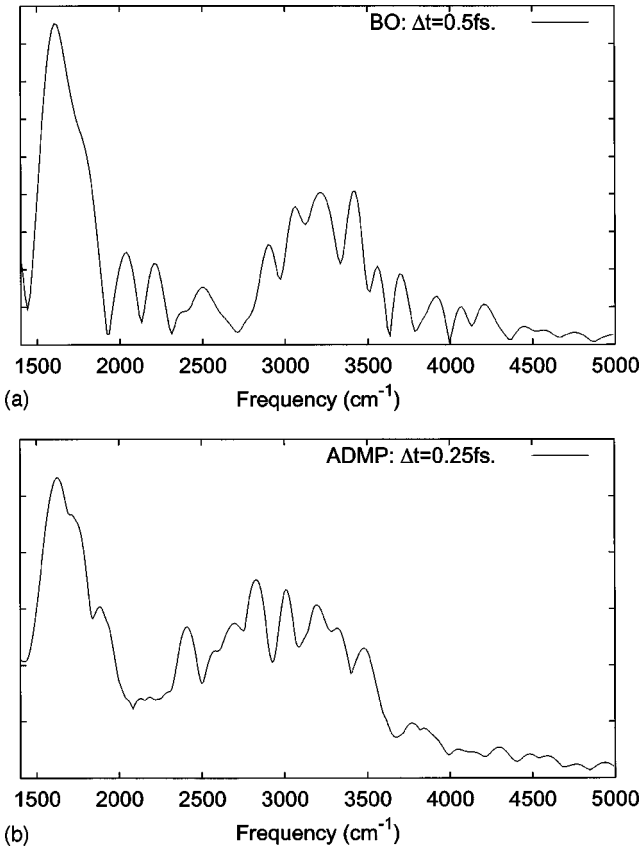

FIG. 7. Fourier transform of the velocity–velocity autocorrelation function showing the vibrational structure of the $Cl^-(H_2O)_{25}$ cluster computed with BO and ADMP using the PBE/3-21G* level of theory.

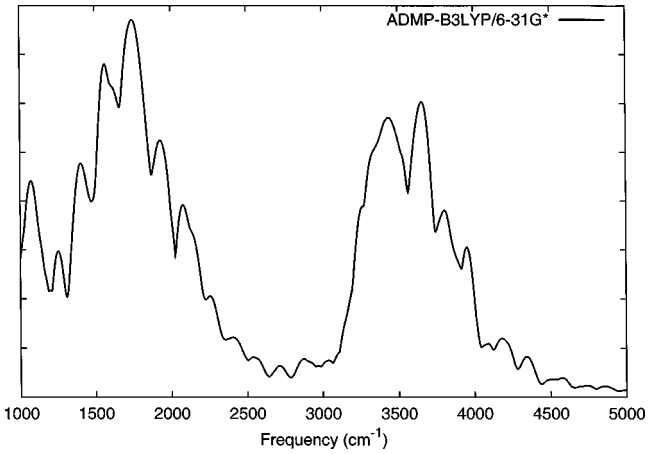

FIG. 8. Fourier transform of the velocity–velocity autocorrelation function showing the vibrational structure of the $Cl^-(H_2O)_{25}$ cluster computed with ADMP using the B3LYP/6-31G* level of theory.

which requires ca. 3 times as much cpu time as a single SCF cycle. Thus, the ADMP approach is 3–4 times faster than the BO method if the step sizes are the same. The earlier discussions demonstrate that the step size for BO cannot be increased by more than a factor of two without significant loss of accuracy. Thus ADMP maintains its computational advantage. Density fitting will accelerate the Fock matrix and gradient evaluation to a similar extent, leaving the timing ratio unchanged. The Coulomb engine approach[88,89] has been used to speed up the Fock matrix calculation within an SCF cycle; a much greater speedup (a factor of 6) can be achieved for the gradients.[90] Hence, the ADMP approach may be as much as 10 times faster than the BO method when the Coulomb engine is used for both Fock matrix and gradient evaluation.

The vibrational properties of chloride water clusters have been well studied both experimentally[91–93] and theoretically.[94] Vibrational properties can be obtained from molecular dynamics data by Fourier transforms of the velocity–velocity autocorrelation function. We studied these using the PBE/3-21G* level of theory for both ADMP and BO dynamics. Because of the relatively short simulation time (1.2 ps for the ADMP trajectory and ~0.5 ps for BO), the Fourier transforms are somewhat noisy, and only the 1400–5000 cm^{-1} range has been considered. To reduce the noise, the ADMP trajectory was broken into four parts, and the transforms averaged; to further control the noise, a smooth window function constructed from the diagonal Fourier space form of the "distributed approximating functional" (DAF)[95,96] was applied to the ADMP and BO velocity–velocity autocorrelation functions before transformation. Some features can be readily distinguished. The PBE/3-21G* results for ADMP and BO are presented in Fig. 7. The sharp peak near 1600–1700 cm^{-1} in both spectra corresponds to the H–O–H bending mode. The broad feature in the 2700–3600 cm^{-1} range extends to lower frequencies than the O–H stretches in the monomer computed at the same level of theory (3304 cm^{-1} and 3448 cm^{-1} at PBE/3-21G*). However, it compares well with the stretch of hydrogen bonded O–H in H_2O–Cl^- and water dimer (2945 cm^{-1} and 3080 cm^{-1}, respectively, at PBE/3-21G*) calculated in the harmonic approximation. Similar redshifts and broadening of the O–H stretching bands for $Cl^-(H_2O)_n$ clusters ($n=1-5$) have been observed experimentally.[89–91] It has been noted in these experiments that in the presence of an Argon matrix the stretch for $Cl^-(H_2O)_1$ occurs at about 3150 cm^{-1}, and in the presence of a CCl_4 matrix the stretch occurs at about 3285 cm^{-1}, compared to 3657 and 3756 cm^{-1} in the water monomer. The redshift is also noted to be comparable for larger clusters and both ADMP and BO studies indicate qualitatively similar results.

In Fig. 8 we present the ADMP results from a ~1 ps simulation at the more accurate B3LYP/6-31G* level of theory. The trajectory was started from the MM3 optimized geometry with a total initial nuclear kinetic energy of 0.1 hartree; the individual atomic velocities being chosen randomly. The initial density matrix velocity was chosen to be zero. As in the case of the PBE/3-21G* simulations, to reduce noise the total trajectory nuclear velocity–velocity autocorrelation function data was split into five parts (of approximately 200 fs each)and each part separately filtered before the respective Fourier transforms were averaged. The resultant Fourier transform (i.e., the density of ro-vibrational states) is shown in Fig. 8 for the 1000–5000 cm^{-1} frequency range (the librational modes at frequencies lower that 1000 cm^{-1} are not well sampled during short simulations). Two O–H stretch peaks at ~3400 and 3600 cm^{-1} can easily be distinguished, showing protons in two different kinds of

chemical environments. One set of protons is in the vicinity of the chloride ion, and is redshifted due to hydrogen bonding with the chloride ion (seen at ~3400 cm^{-1} in Fig. 8). This redshifted frequency maybe compared to the harmonic vibrational frequency of 3379 cm^{-1} obtained from a separate B3LYP/6-31G* calculation of H_2O–Cl^-. The second set of protons, corresponding to the O–H stretch at 3600 cm^{-1}, are not significantly perturbed by the Cl^- as can be seen from the similarity of their O–H stretching frequencies to that in bulk-water (~3700 cm^{-1}) and water dimer (3620–3833 cm^{-1} calculated at B3LYP/6-31G*). ADMP calculations with larger basis sets are currently underway to study these redshifts further.[97] It is already clear that ADMP is powerful and efficient computational tool for studying molecular dynamics in chemical systems.

VII. CONCLUSIONS

In the present paper, we have compared the performance of two approaches to *ab initio* molecular dynamics: the extended Lagrangian formalism with propagation of the density matrix using atom centered Gaussian functions (ADMP), and the Born–Oppenheimer (BO) method in which the density is converged at each nuclear configuration instead of being propagated. Three test cases were considered: photodissociation of formaldehyde, three-body fragmentation of glyoxal, and a cluster of chloride ion with 25 water molecules. In all cases, energy conservation and adiabaticity were maintained very well, and good agreement was found between the two trajectory methods for dynamical properties such as product energy distributions and vibrational structure.

The effect of changing the magnitude of the fictitious mass on the molecular properties was studied in an ionic system. For NaCl monomer, the vibrational period remains quantitatively the same over a range of values for the fictitious mass parameter in our ADMP formalism. This is particularly encouraging in light of a rather disturbing observation made in Ref. 29, where the authors find that the vibrational frequencies of ionic systems vary with changes in fictitious mass parameter in the standard plane-wave implementation of the Car–Parrinello scheme.

The present implementation of the extended Lagrangian approach is 3–4 times faster than the Born–Oppenheimer method for larger systems. Inclusion of the Coulomb engine for the gradient of the energy with respect to the nuclei will improve this ratio substantially.

ACKNOWLEDGMENTS

This work was supported by the National Science Foundation (Grants Nos. CHE-9982156, CHE-9874005, and CHE-0131157), the Office of Naval Research (GAV) and Gaussian, Inc. An allocation of computer time from the Center of High Performance Computing at the University of Utah is gratefully acknowledged.

[1] K. Bolton, W. L. Hase, and G. H. Peslherbe, in *Modern Methods for Multidimensional Dynamics Computation in Chemistry*, edited by D. L. Thompson (World Scientific, Singapore, 1998), pp. 143.
[2] R. Car and M. Parrinello, Phys. Rev. Lett. **55**, 2471 (1985).
[3] M. E. Tuckerman, P. J. Ungar, T. vonRosenvinge, and M. L. Klein, J. Phys. Chem. **100**, 12878 (1996).
[4] D. K. Remler and P. A. Madden, Mol. Phys. **70**, 921 (1990).
[5] M. C. Payne, M. P. Teter, D. C. Allan, T. A. Arias, and J. D. Joannopoulos, Rev. Mod. Phys. **64**, 1045 (1992).
[6] E. Deumens, A. Diz, R. Longo, and Y. Ohrn, Rev. Mod. Phys. **66**, 917 (1994).
[7] D. Marx and J. Hutter, in *Modern Methods and Algorithms of Quantum Chemistry*, edited by J. Grotendorst (John vonNeumann Institute for Computing, Julich, 2000), Vol. 1, pp. 301.
[8] H. C. Andersen, J. Chem. Phys. **72**, 2384 (1980).
[9] M. Parrinello and A. Rahman, Phys. Rev. Lett. **45**, 1196 (1980).
[10] G. Lippert, J. Hutter, and M. Parrinello, Theor. Chem. Acc. **103**, 124 (1999).
[11] G. Lippert, J. Hutter, and M. Parrinello, Mol. Phys. **92**, 477 (1997).
[12] H. B. Schlegel, J. M. Millam, S. S. Iyengar, G. A. Voth, A. D. Daniels, G. E. Scuseria, and M. J. Frisch, J. Chem. Phys. **114**, 9758 (2001).
[13] S. S. Iyengar, H. B. Schlegel, J. M. Millam, G. A. Voth, G. E. Scuseria, and M. J. Frisch, J. Chem. Phys. **115**, 10291 (2001).
[14] G. E. Scuseria, J. Phys. Chem. A **103**, 4782 (1999).
[15] S. S. Iyengar, K. Kudin, H. B. Schlegel, J. M. Millam, G. A. Voth, G. E. Scuseria, and M. J. Frisch (unpublished).
[16] N. Rega, S. S. Iyengar, G. A. Voth, H. B. Schlegel, G. E. Scuseria, and M. J. Frisch (unpublished).
[17] S. S. Iyengar, T. J. F. Day, and G. A. Voth, J. Am. Chem. Soc. (submitted).
[18] Charged systems are generally treated in plane-wave CP calculations by introducing a potential to screen the Coulomb interaction and by increasing the size of the periodic cell.
[19] R. N. Barnett and U. Landman, Phys. Rev. B **48**, 2081 (1993).
[20] S. Nose, J. Chem. Phys. **81**, 511 (1984).
[21] W. G. Hoover, Phys. Rev. A **31**, 1695 (1985).
[22] M. E. Tuckerman and M. Parrinello, J. Chem. Phys. **101**, 1316 (1994).
[23] D. A. Gibson, I. V. Ionova, and E. A. Carter, Chem. Phys. Lett. **240**, 261 (1995).
[24] B. Hartke and E. A. Carter, J. Chem. Phys. **97**, 6569 (1992).
[25] B. Hartke and E. A. Carter, Chem. Phys. Lett. **189**, 358 (1992).
[26] P. Pulay, G. Fogarasi, F. Pang, and J. E. Boggs, J. Am. Chem. Soc. **101**, 2550 (1979).
[27] D. A. Gibson and E. A. Carter, J. Phys. Chem. **97**, 13429 (1993).
[28] G. Martyna, C. Cheng, and M. L. Klein, J. Chem. Phys. **95**, 1318 (1991).
[29] P. Tangney and S. Scandolo, J. Chem. Phys. **116**, 14 (2002).
[30] J. M. Millam and G. E. Scuseria, J. Chem. Phys. **106**, 5569 (1997).
[31] R. McWeeny, Rev. Mod. Phys. **32**, 335 (1960).
[32] W. C. Swope, H. C. Andersen, P. H. Berens, and K. R. Wilson, J. Chem. Phys. **76**, 637 (1982).
[33] M. E. Tuckerman and M. Parrinello, J. Chem. Phys. **101**, 1302 (1994).
[34] D. K. Hoffman, M. Arnold, and D. J. Kouri, J. Phys. Chem. **97**, 1110 (1993).
[35] D. A. Micha, J. Phys. Chem. A **103**, 7562 (1999).
[36] I. Daubechies, *Ten Lectures in Wavelets* (SIAM, Philadelphia, PA, 1992).
[37] A. Grossmann and J. Morlet, SIAM (Soc. Ind. Appl. Math.) J. Math. Anal. **15**, 723 (1984).
[38] R. I. McLachlan and P. Atela, Nonlinearity **5**, 541 (1992).
[39] M. Tuckerman, B. J. Berne, and G. J. Martyna, J. Chem. Phys. **97**, 1990 (1992).
[40] A. K. Mazur, J. Comput. Phys. **136**, 354 (1997).
[41] P. L. Houston and C. B. Moore, J. Chem. Phys. **65**, 757 (1976).
[42] P. Ho, D. J. Bamford, R. J. Buss, T. T. Lee, and C. B. Moore, J. Chem. Phys. **76**, 3630 (1982).
[43] C. B. Moore and J. C. Weisshaar, Annu. Rev. Phys. Chem. **34**, 525 (1983).
[44] R. D. van Zee, M. F. Foltz, and C. B. Moore, J. Chem. Phys. **99**, 1664 (1993).
[45] R. D. van Zee, C. D. Pibel, T. J. Butenhoff, and C. B. Moore, J. Chem. Phys. **97**, 3235 (1992).
[46] D. Debarre, M. Lefrebvre, M. Péalat, and J.-P. E. Taran, J. Chem. Phys. **83**, 4476 (1985).
[47] D. J. Bamford, S. V. Filseth, M. F. Foltz, J. W. Hepburn, and C. B. Moore, J. Chem. Phys. **82**, 3032 (1985).
[48] D. R. Guyer, W. F. Polik, and C. B. Moore, J. Chem. Phys. **84**, 6519 (1986).
[49] T. J. Butenhoff, K. L. Carleton, M. C. Chuang, and C. B. Moore, J. Chem. Soc., Faraday Trans. 2 **85**, 1155 (1989).
[50] T. J. Butenhoff, K. L. Carleton, and C. B. Moore, J. Chem. Phys. **92**, 377 (1990).

[51] K. L. Carleton, T. J. Butenhoff, and C. B. Moore, J. Chem. Phys. **93**, 3907 (1990).
[52] J. D. Goddard and H. F. Schaefer, III J. Chem. Phys. **70**, 5117 (1979).
[53] L. B. Harding, H. B. Schlegel, R. Krishnan, and J. A. Pople, J. Phys. Chem. **84**, 3394 (1980).
[54] J. D. Goddard, Y. Yamaguchi, and H. F. Schaefer III, J. Chem. Phys. **75**, 3459 (1981).
[55] G. F. Adams, G. D. Bent, R. J. Bartlett, and G. D. Purvis, J. Chem. Phys. **75**, 834 (1981).
[56] M. Dupuis, W. A. Lester, B. H. Lengsfield, and B. Liu, J. Chem. Phys. **79**, 6167 (1983).
[57] M. J. Frisch, J. S. Binkley, and H. F. Schaefer, III J. Chem. Phys. **81**, 1882 (1984).
[58] G. E. Scuseria and H. F. Schaefer, III J. Chem. Phys. **90**, 3629 (1989).
[59] H. Nakano, K. Nakayama, K. Hirao, and M. Dupuis, J. Chem. Phys. **106**, 4912 (1997).
[60] D. Feller, M. Dupuis, and B. C. Garrett, J. Chem. Phys. **113**, 218 (2000).
[61] J. Troe, J. Phys. Chem. **88**, 4375 (1984).
[62] R. Schinke, Annu. Rev. Phys. Chem. **39**, 39 (1988).
[63] W. H. Miller, R. Hernandez, N. C. Handy, D. Jayatilaka, and A. Willetts, Chem. Phys. Lett. **172**, 62 (1990).
[64] W. L. Hase and K. N. Swamy, Chem. Phys. Lett. **92**, 371 (1982).
[65] Y. T. Chang, C. Minichino, and W. H. Miller, J. Chem. Phys. **96**, 4341 (1992).
[66] G. H. Peslherbe and W. L. Hase, J. Chem. Phys. **104**, 7882 (1996).
[67] B. J. Sung and M. S. Kim, J. Chem. Phys. **113**, 3098 (2000).
[68] W. Chen, W. L. Hase, and H. B. Schlegel, Chem. Phys. Lett. **228**, 436 (1994).
[69] X. S. Li, J. M. Millam, and H. B. Schlegel, J. Chem. Phys. **113**, 10062 (2000).
[70] M. J. Frisch, G. W. Trucks, H. B. Schlegel, G. E. Scuseria *et al.*, Gaussian 01, Development Version (Revision B.02), Gaussian, Inc., Pittsburgh, PA, 2002.
[71] J. M. Millam, V. Bakken, W. Chen, W. L. Hase, and H. B. Schlegel, J. Chem. Phys. **111**, 3800 (1999).
[72] V. Bakken, J. M. Millam, and H. B. Schlegel, J. Chem. Phys. **111**, 8773 (1999).
[73] S. S. Iyengar, G. A. Voth, H. B. Schlegel, J. M. Millam, G. E. Scuseria, and M. J. Frisch (unpublished).
[74] L. M. Dobeck, H. M. Lambert, W. Kong, P. J. Pisano, and P. L. Houston, J. Phys. Chem. A **103**, 10312 (1999).
[75] J. W. Hepburn, R. J. Buss, L. J. Butler, and Y. T. Lee, J. Phys. Chem. **87**, 3638 (1983).
[76] I. Burak, J. W. Hepburn, N. Sivakumar, G. E. Hall, G. Chawla, and P. L. Houston, J. Chem. Phys. **86**, 1258 (1987).
[77] Y. Osamura and H. F. Schaefer, III J. Chem. Phys. **74**, 4576 (1981).
[78] Y. Osamura, H. F. Schaefer, III M. Dupuis, and W. A. Lester, J. Chem. Phys. **75**, 5828 (1981).
[79] G. E. Scuseria and H. F. Schaefer, III J. Am. Chem. Soc. **111**, 7761 (1989).
[80] X. S. Li and H. B. Schlegel, J. Chem. Phys. **114**, 8 (2001).
[81] D. M. Koch, N. N. Khieu, and G. H. Peslherbe, J. Phys. Chem. A **105**, 3598 (2001).
[82] K. Saito, T. Kakumoto, and I. Murakami, J. Phys. Chem. **88**, 1182 (1984).
[83] X. S. Li, J. M. Millam, and H. B. Schlegel, J. Chem. Phys. **114**, 8897 (2001).
[84] X. S. Li, J. M. Millam, and H. B. Schlegel, J. Chem. Phys. **115**, 6907 (2001).
[85] J. P. Perdew, K. Burke, and Y. Wang, Phys. Rev. B **54**, 16533 (1996).
[86] J. P. Perdew, K. Burke, and M. Ernzerhof, Phys. Rev. Lett. **77**, 3865 (1996); Phys. Rev. Lett. **78**, 1396 (1997).
[87] L. X. Dang and B. M. Pettitt, J. Phys. Chem. **91**, 3349 (1987).
[88] G. R. Ahmadi and J. Almlof, Chem. Phys. Lett. **246**, 364 (1995).
[89] Y. Y. Shao and M. Head-Gordon, Chem. Phys. Lett. **323**, 425 (2000).
[90] Y. H. Shao, C. A. White, and M. Head-Gordon, J. Chem. Phys. **114**, 6572 (2001).
[91] J. H. Choi, K. T. Kuwata, Y. B. Cao, and M. Okumura, J. Phys. Chem. A **102**, 503 (1998).
[92] P. Ayotte, G. H. Weddle, J. Kim, and M. A. Johnson, J. Am. Chem. Soc. **120**, 12361 (1998).
[93] P. Ayotte, S. B. Nielsen, G. H. Weddle, M. A. Johnson, and S. S. Xantheas, J. Phys. Chem. A **103**, 10665 (1999).
[94] G. K. Schenter, B. C. Garrett, and G. A. Voth, J. Chem. Phys. **113**, 5171 (2000).
[95] D. K. Hoffman and D. J. Kouri, in *Proceedings of 3rd International Conference Mathematical and Numerical Aspects of Wave Propagation*, edited by G. Cohen (SIAM, Philadelphia, PA, 1995), p. 56.
[96] S. S. Iyengar, D. J. Kouri, and D. K. Hoffman, Theor. Chem. Acc. **104**, 471 (2000).
[97] S. S. Iyengar, G. A. Voth, H. B. Schlegel, G. E. Scuseria, and M. J. Frisch (unpublished).